Spherical-wave intensity diffraction tomography

Greg Gbur

Department of Physics and Astronomy, Free University, De Boelelaan 1081, 1081 HV Amsterdam, The Netherlands

Mark A. Anastasio, Yin Huang, and Daxin Shi

Department of Biomedical Engineering, Illinois Institute of Technology, Chicago, Illinois 60616

Received January 27, 2004; revised manuscript received August 20, 2004; accepted September 1, 2004

An extension of the recently developed method of intensity diffraction tomography is derived that assumes that the probing field is a spherical wave produced by a point source sufficiently far from the scatterer. A discussion of the method and numerical reconstructions of a simulated three-dimensional scattering object are presented.

OCIS codes: 110.6960, 290.3200, 120.5050.

1. INTRODUCTION

Diffraction tomography (DT)[1] is now a well-established method for reconstructing the three-dimensional (3D) refractive index of a weakly scattering object by measurements of the field scattered by the object. One of the most significant challenges in applying the method with optical fields is that it requires both amplitude and phase measurements of the scattered field, and phase measurements of optical fields generally present considerable practical difficulties.

Some recent theoretical results have demonstrated that DT may be performed with intensity measurements alone.[2,3] This new method, to be referred to as intensity diffraction tomography (I-DT), uses plane waves as the probing fields and replaces phase measurements with multiple measurements of the diffracted-field intensity along the direction of propagation. In many practical experiments, however, the probing field may be a spherical wave produced by a point source located a finite distance away from the scatterer. Some years ago Devaney[4] reformulated DT for this case, assuming that the point source was located sufficiently far from the scattering object. Specifically, a generalized Fourier diffraction projection (FDP) theorem was derived that provided a linear relationship between the measured scattered field (or complex phase perturbation) and the scattering potential of the object.

In this paper we demonstrate that the previously developed plane-wave I-DT method can be extended to the spherical-wave formulation that was considered by Devaney. As in the plane-wave I-DT method, explicit phase measurements are replaced by measurements of the diffracted-wave-field intensity on different parallel planes at each tomographic view angle. In Section 2 we review those results from plane-wave DT and I-DT that are necessary for our analysis. In Section 3 the new spherical-wave I-DT method is derived and investigated analytically. Sections 4 and 5 contain numerical reconstructions of a simulated 3D scattering object and concluding remarks, respectively.

2. REVIEW OF PLANE-WAVE DIFFRACTION TOMOGRAPHY AND INTENSITY DIFFRACTION TOMOGRAPHY

A. Plane-Wave Diffraction Tomography

Here we consider the classical scanning geometry of plane-wave DT that is illustrated in Fig. 1. A monochromatic scalar plane wave $U_i(\mathbf{r}) = \exp[ik\mathbf{s}_0 \cdot \mathbf{r}]$, where $\mathbf{r} \equiv (x, y, z)$, $k = \omega/c$ is the wave number, and time dependence $\exp(-i\omega t)$ is assumed, is incident on an object occupying a volume V with a (generally) complex index of refraction $n(\mathbf{r})$. The unit vectors $\mathbf{s}_1$, $\mathbf{s}_2$, and $\mathbf{s}_0$ indicate the directions of the positive x, y, and z axes, respectively. If the scattering is sufficiently weak (as is usually assumed in diffraction tomography experiments), the field beyond the scatterer may be expressed in the form of the first Rytov approximation (Ref. 5, Sec. 13.5),

$$U(\mathbf{r}) \approx U_i(\mathbf{r})\exp[\psi(\mathbf{r})], \tag{1}$$

where

$$\psi(\mathbf{r}) = \frac{1}{U_i(\mathbf{r})}\int_V F(\mathbf{r}')\frac{\exp[ik|\mathbf{r}-\mathbf{r}'|]}{|\mathbf{r}-\mathbf{r}'|}U_i(\mathbf{r}')\mathrm{d}^3r' \tag{2}$$

is a complex phase perturbation of the incident field, and

$$F(\mathbf{r}) = \frac{k^2}{4\pi}[n^2(\mathbf{r}) - 1] \tag{3}$$

is referred to as the scattering potential of the object. Let

$$\tilde{F}(\mathbf{K}) = \frac{1}{(2\pi)^3}\int_V F(\mathbf{r}')\exp[-i\mathbf{K}\cdot\mathbf{r}']\mathrm{d}^3r' \tag{4}$$

denote the 3D Fourier transform of $F(\mathbf{r})$ and define

$$\tilde{F}[u, v, (w-k)] \equiv \tilde{F}(u\mathbf{s}_1 + v\mathbf{s}_2 + (w-k)\mathbf{s}_0). \tag{5}$$

By use of the Weyl representation of the free-space Green's function (Ref. 6, Sec. 3.2), $\psi(\mathbf{r})$ may be rewritten in the form

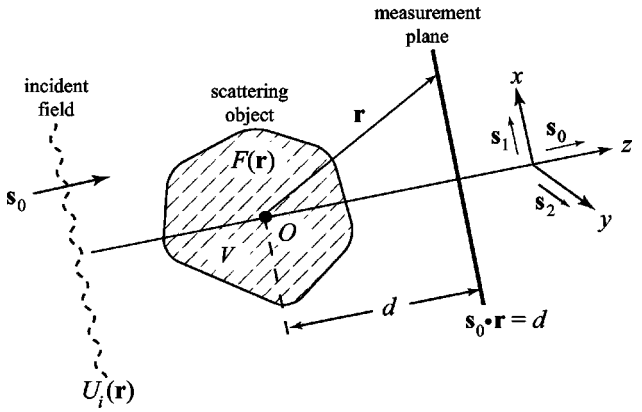

Fig. 1. Illustration of the configuration for weak scattering and diffraction tomography.

$$\psi(x, y, z) = i(2\pi)^2 \int\int \frac{1}{w} \tilde{F}[u, v, (w - k)] \times \exp[i(w - k)z]\exp[i(ux + vy)]\mathrm{d}u\,\mathrm{d}v, \tag{6}$$

where

$$w = \begin{cases} (k^2 - u^2 - v^2)^{1/2} & \text{when } u^2 + v^2 \leqslant k^2 \\ i(u^2 + v^2 - k^2)^{1/2} & \text{when } u^2 + v^2 > k^2. \end{cases} \tag{7}$$

Equation (6) relates the complex phase perturbation $\psi(\mathbf{r})$ of the incident field to the 3D Fourier components of the scattering potential. This relation can be put in a simpler form by considering the two-dimensional Fourier transform of $\psi(\mathbf{r})$ in the measurement plane that is given by

$$\hat{\psi}(u, v; z) = \frac{1}{(2\pi)^2} \int\int \psi(x, y, z) \times \exp[-i(ux + vy)]\mathrm{d}x\mathrm{d}y. \tag{8}$$

On substituting from Eq. (6) into Eq. (8) and evaluating the integrals, it follows that

$$\hat{\psi}(u, v; z) = \frac{(2\pi)^2 i}{w} \tilde{F}[u, v, (w - k)]\exp[i(w - k)z]. \tag{9}$$

Equation (9) is the FDP theorem of plane-wave DT. It relates the two-dimensional Fourier transform of the phase perturbation on a measurement plane to the 3D Fourier transform of the scattering potential. By use of measurements for multiple directions of the incident field, a low-pass-filtered reconstruction of the scattering potential may be obtained. A number of algorithms have been developed to reconstruct $F(\mathbf{r})$ efficiently in this manner.[7,8]

B. Plane-Wave Intensity Diffraction Tomography

It is not difficult to see that the intensity of the field in a single measurement plane does not contain enough information to reconstruct the scattering object. If we define an intensity data function $D_I(\mathbf{r})$ by the expression,

$$D_I(\mathbf{r}) \equiv \log[I(\mathbf{r})/I_i(\mathbf{r})] = \psi(\mathbf{r}) + \psi^*(\mathbf{r}), \tag{10}$$

where $I(\mathbf{r}) = |U(\mathbf{r})|^2$ and $I_i(\mathbf{r}) = |U_i(\mathbf{r})|^2$, one can show that the two-dimensional Fourier transform of this data function in a plane of constant z is given by the expression

$$\hat{D}_I(u, v; z) = i\frac{(2\pi)^2}{|w|^2}\{w^*\tilde{F}[u, v, (w - k)]\exp[i(w - k)z] - w[\tilde{F}[-u, -v, (w - k)]]^* \exp[-i(w^* - k)z]\}. \tag{11}$$

It is clear that in a given z plane, different components of $\tilde{F}(\mathbf{K})$ are mixed together in a way such that their individual contributions are not determinable, save possibly in special cases of high symmetry.

The plane-wave I-DT method consists in defining a data function of the form

$$\hat{D}_\Delta(u, v; d) \equiv \frac{\hat{D}_I(u, v; d) - \hat{D}_I(u, v; d + \Delta)\exp[i(w - k)\Delta]}{\Delta}, \tag{12}$$

where intensity data are employed from a pair of measurement planes spaced by a distance Δ (see Fig. 2). It is to be noted that the Δ in the denominator of Eq. (12) is a formal convention, chosen to give the data function a nonzero value in the limit $\Delta \to 0$; i.e.,

$$\lim_{\Delta\to 0} \hat{D}_\Delta(u, v; d) = -\frac{\partial}{\partial z}\hat{D}_I(u, v; z)\big|_{z=d} - i(w - k)\hat{D}_I(u, v; d). \tag{13}$$

This data function is comparable to that used in the phase reconstruction problem of the so-called transport-of-intensity equation.[9] On substituting from Eq. (11) into Eq. (12), it follows that

$$\hat{D}_\Delta(u, v; d) = \frac{(2\pi)^2 i}{w\Delta}\tilde{F}[u, v, (w - k)]\exp[i(w - k)d] \times \{1 - \exp[2i(w - k)\Delta]\}. \tag{14}$$

This equation can be viewed as an FDP theorem for plane-wave I-DT. On comparison with Eq. (9), it can be seen that the two equations are nearly identical except for the presence of an additional Δ-dependent term in the I-DT theorem. Intensity diffraction tomography there-

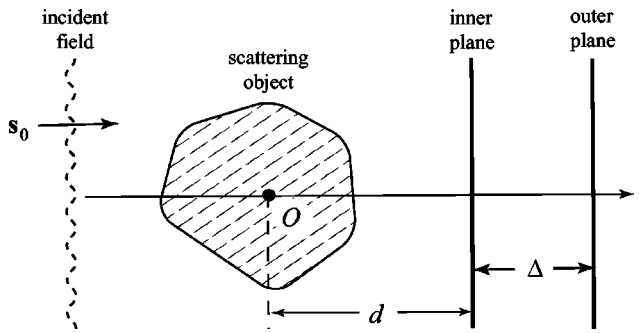

Fig. 2. Illustration of the configuration for plane-wave I-DT.

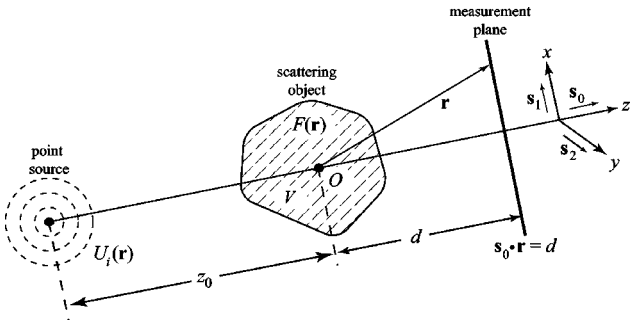

Fig. 3. Illustration of the configuration for spherical-wave DT.

fore replaces phase measurements of the scattered field with additional intensity measurements. A physical understanding of this method and some of its limitations are discussed in Refs. 2 and 3. One obvious difficulty arises as a result of the factor in curly braces in Eq. (14): The data function vanishes for $u = v = 0$. An identical difficulty appears in spherical-wave I-DT and will be discussed below.

3. SPHERICAL-WAVE INTENSITY DIFFRACTION TOMOGRAPHY

In tomographic experiments, it is often easier to implement a configuration in which the incident field is a diverging spherical wave. We now describe the extension of I-DT to the spherical-wave configuration.

We consider a measurement configuration where the incident field is a spherical wave generated from a point on the z-axis $\mathbf{r}_0 = (0, 0, -z_0)$ (see Fig. 3). The incident field takes on the form

$$U_i(\mathbf{r}) = \frac{\exp[ik|\mathbf{r} - \mathbf{r}_0|]}{|\mathbf{r} - \mathbf{r}_0|}, \tag{15}$$

and the complex phase perturbation is again given by Eq. (2).

It is assumed that both the source point $\mathbf{r}_0$ and the observation point $\mathbf{r}$ are sufficiently far from the scattering object that the paraxial approximation may be used for both the incident field and the spherical wave in Eq. (2). It is also assumed that the structure of the scattering object is such that the scattering is primarily in the forward z direction. Under these assumptions, Devaney showed [Ref. 4, Eq. (24)] that the complex phase $\psi(\mathbf{r})$ may be expressed in the form

$$\psi(\mathbf{r}) \approx \frac{1}{U_i(\mathbf{r})} \frac{\exp[ikz_0]}{z_0} \exp[ik\rho^2/2(z + z_0)] \times \int_V F(\mathbf{r}') \exp[ikz'] \frac{\exp[ik|\mathbf{r}_a - \mathbf{r}_b|]}{|\mathbf{r}_a - \mathbf{r}_b|} \mathrm{d}^3 r', \tag{16}$$

where $\boldsymbol{\rho} = (x, y)$ is a vector in the transverse plane with magnitude $\rho = (x^2 + y^2)^{1/2}$,

$$\mathbf{r}_a = (\alpha\boldsymbol{\rho}, z), \tag{17}$$

$$\mathbf{r}_b = (\boldsymbol{\rho}'/\alpha, z'), \tag{18}$$

and

$$\alpha \equiv \left(\frac{z_0}{z + z_0}\right)^{1/2} < 1. \tag{19}$$

With use of the paraxial approximation for the incident field,

$$U_i(\mathbf{r}) \approx \frac{1}{|\mathbf{r} - \mathbf{r}_0|} \exp[ik(z + z_0)] \exp[ik\rho^2/2(z + z_0)], \tag{20}$$

relation (16) simplifies to the form

$$\psi(\mathbf{r}) = \frac{|\mathbf{r} - \mathbf{r}_0|}{z_0} \exp[-ikz] \times \int_V F(\mathbf{r}') \exp[ikz'] \frac{\exp[ik|\mathbf{r}_a - \mathbf{r}_b|]}{|\mathbf{r}_a - \mathbf{r}_b|} \mathrm{d}^3 r'. \tag{21}$$

Let us define a modified phase function as

$$Q(\mathbf{r}) = \frac{\psi(\mathbf{r})}{|\mathbf{r} - \mathbf{r}_0|}. \tag{22}$$

The spherical wave in Eq. (21) containing the vectors $\mathbf{r}_a$ and $\mathbf{r}_b$ may be expanded by using the Weyl representation, and then following steps analogous to those described in Section 2 we may derive the relation

$$\hat{Q}[u, v; z] = \frac{1}{z_0 w_\alpha} \frac{(2\pi)^2 i}{\alpha^2} \tilde{F}[u/\alpha^2, v/\alpha^2, w_\alpha - k] \times \exp[i(w_\alpha - k)z], \tag{23}$$

where

$$w_\alpha \equiv [k^2 - (u/\alpha)^2 - (v/\alpha)^2]^{1/2} \tag{24}$$

and $\hat{Q}$ is the two-dimensional spatial Fourier transform of Q in the transverse plane. This formula demonstrates that in spherical-wave DT, as in plane-wave DT, the Fourier components of the data function Q on the plane are

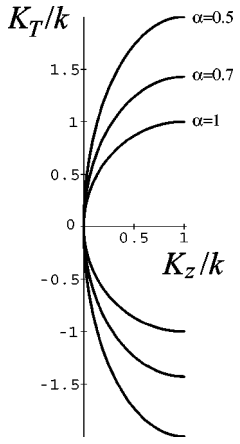

Fig. 4. Fourier components available when spherical-wave tomography is used for different values of the parameter α. Here K_z is the z-component of the wavevector in Fourier space, and K_T is the magnitude of the transverse part of the wavevector in Fourier space, i.e., $K_T \equiv (K_x^2 + K_y^2)^{1/2}$.

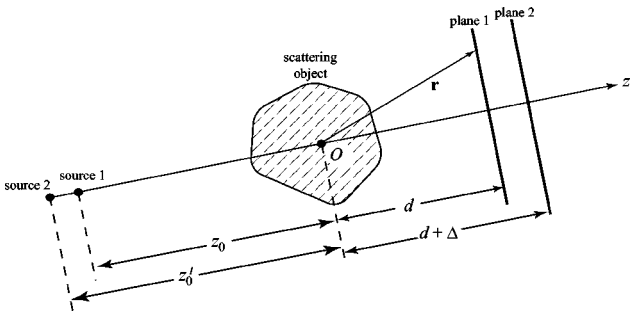

Fig. 5. Illustration of the configuration for spherical-wave I-DT.

directly related to the 3D Fourier components of the scattering potential. The available components are illustrated in Fig. 4 for various values of the parameter α; it is to be noted that $\alpha = 1$ is the usual plane-wave result.

Following the I-DT analysis described in Section 2, we define a new spherical-wave intensity data function of the form

$$D_S(\mathbf{r}, z_0) \equiv \frac{1}{|\mathbf{r} - \mathbf{r}_0|}\log[I(\mathbf{r})/I_i(\mathbf{r})], \tag{25}$$

If the measurement planes are widely spaced, however (for instance, to get better measurements of the low-spatial-frequency components as discussed below), a method is required that can reconstruct exactly the Fourier components of the scattering potential. A key observation is that the change in α that occurs by increasing the measurement plane distance by Δ can be compensated for by changing the position of the source to a new axial position $-z_0'$. By requiring that the value of α remain unchanged for the second intensity measurement, one finds readily that

$$z_0' = \frac{(z + \Delta)z_0}{z}. \tag{27}$$

This configuration is illustrated in Fig. 5. It should be noted that, according to Eq. (27), the second source position z_0' is *farther* away from the scattering object than is the first source position z_0.

With this new measurement configuration, we define a spherical-wave I-DT data function as

$$\hat{D}_\Delta^S(u, v; d) = \frac{z_0\hat{D}_S(u, v; d, z_0) - z_0'\hat{D}_S(u, v; d + \Delta, z_0')\exp[i(w_\alpha - k)\Delta]}{\Delta}. \tag{28}$$

and straightforward calculation shows that the two-dimensional Fourier transform of this data function in the plane $z = d$ has the form

$$\hat{D}_S(u, v; d, z_0) = \frac{(2\pi)^2 i}{z_0 w_\alpha \alpha^2}\{\tilde{F}[u/\alpha^2, v/\alpha^2, (w_\alpha - k)]\exp[i(w_\alpha - k)d] - [\tilde{F}[-u/\alpha^2, -v/\alpha^2, (w_\alpha - k)]]^* \exp[-i(w_\alpha - k)d]\}. \tag{26}$$

Similarly to the plane-wave case, one might attempt to utilize Eq. (26), along with the two intensity measurements on the planes $z = d$ and $z = d + \Delta$, to establish a system of two equations with two unknowns that can be solved for $\tilde{F}[u/\alpha^2, v/\alpha^2, (w_\alpha - k)]$. However, this is not possible if the source-to-object distance z_0 is kept constant, because the intensity measurements acquired on the $z = d$ and $z = d + \Delta$ planes will be related to different spatial-frequency components of $F(\mathbf{r})$ through Eq. (26) (because the values of α will be distinct).

There exist at least two possibilities for circumventing this problem. The simplest of these is to note that α depends very weakly on z, i.e., $\alpha = [z_0/(z + z_0)]^{1/2}$. If the spacing Δ between the selected pair of measurement planes is appreciably less than $z_0 + d$, then α will be effectively the same on the two measurement planes, and we may perform a method essentially identical to the methods described in Refs. 2 and 3.

On substituting from Eq. (26) into Eq. (28), one finds that

$$\hat{D}_\Delta^S(u, v; d) = \frac{(2\pi)^2 i}{\alpha^2 w_\alpha \Delta}\tilde{F}[u/\alpha^2, v/\alpha^2, (w_\alpha - k)]\{1 - \exp[2i(w_\alpha - k)\Delta]\}\exp[i(w_\alpha - k)d]. \tag{29}$$

This expression is nearly identical to Eq. (14), the only significant changes being the contraction of u and v by α^2, as in ordinary spherical-wave diffraction tomography, and the replacement of w by w_α. Equation (29) can be viewed as the FDP theorem for spherical-wave I-DT, because it relates the Fourier components of the intensity on two measurement planes to the 3D Fourier components of the scattering potential. It is to be noted that the components of $\tilde{F}$ that satisfy

$$2(w_\alpha - k)\Delta = 2n\pi, \tag{30}$$

where n is an integer, cannot be determined through Eq. (29).

Interestingly, the Fourier components of $F(\mathbf{r})$ may also be determined from intensity measurements even if the source–object spacing z_0 is held fixed, albeit at a significant increase in computational complexity. We discuss such possibilities in Appendix A.

4. NOISE PROPERTIES

To understand some basic statistical properties of the spherical-wave I-DT method, we assume that the inten-

sity measurements are corrupted by some source of stochastic noise and treat the functions $\hat{\mathbf{D}}_{\Delta}^{\mathbf{S}}(u, v; d)$ and $\tilde{\mathbf{F}}[u/\alpha^2, v/\alpha^2, (w_\alpha - k)]$ as random variables. (Here and in the following, a boldface font will denote a random variable.) By use of Eq. (29) one finds readily that

$$\mathrm{Var}\{\tilde{\mathbf{F}}[u/\alpha^2, v/\alpha^2, (w_\alpha - k)]\} = \frac{\alpha^4 w_\alpha^2 \Delta^2}{(2\pi)^4} \frac{\mathrm{Var}\{\hat{\mathbf{D}}_{\Delta}^{\mathbf{S}}(u, v; d)\}}{2[1 - \cos(2(w_\alpha - k)\Delta)]}, \quad (31)$$

where $\mathrm{Var}\{\cdot\}$ denotes the variance of a random variable. Equation (31) describes how $\mathrm{Var}\{\tilde{\mathbf{F}}[u/\alpha^2, v/\alpha^2, (w_\alpha - k)]\}$ depends on $\mathrm{Var}\{\hat{\mathbf{D}}_{\Delta}^{\mathbf{S}}(u, v; d)\}$ (determined from the statistics of the measured data), wavenumber k, detector spacing Δ, and geometry parameter α. This equation demonstrates that the variance in the estimate $\mathrm{Var}\{\tilde{\mathbf{F}}[u/\alpha^2, v/\alpha^2, (w_\alpha - k)]\}$ becomes exceedingly large for components (u, v) near the singular points (u_s, v_s) that satisfy $2(w_\alpha - k)\Delta = 2n\pi$, which includes the zero-frequency component $(u_s = 0, v_s = 0)$ for the case $n = 0$. In practice, it is therefore advisable to estimate $\tilde{F}$ only for $(u, v) \neq (0, 0)$ that have values smaller than those defined by the $n = 1$ case of Eq. (30). It is also very important to estimate accurately the low-frequency components of $\tilde{\mathbf{F}}$ in order to avoid significant distortions and nonuniform background structures in the reconstructed scattering potential $\mathbf{F}(\mathbf{r})$. It is evident that for (u, v) near $(0, 0)$, the value of the denominator in Eq. (31) increases as the value of Δ increases, thereby reducing the variance of the estimate. Therefore the variance of low-frequency components of $\tilde{\mathbf{F}}$ can be reduced by use of scanning geometries that employ sufficiently large values for the detector spacing Δ. In Section 5, we demonstrate numerically the regularizing effect that suitable choices for Δ can have in spherical-wave I-DT.

It is to be noted that additional measurement planes (measurements for more values of Δ) could be used to obtain better estimates of $\tilde{\mathbf{F}}$ near $(0, 0)$ and near the other singular points (u_s, v_s). This possibility is discussed briefly for the plane-wave I-DT case in Ref. 10.

5. NUMERICAL RESULTS

We performed simulation studies to validate and demonstrate the spherical-wave I-DT reconstruction method.

A. Simulation Data

Noiseless and noisy scattered field data were generated from a simulated (weakly) scattering object that was composed of three uniform spherical scatterers with radii of 1, 1.2, and 1.5 (arbitrary units) that were centered at the coordinates $(x, y, z) = (13.5, 13.5, 9)$, $(-13.5, -13.5, 0)$ and $(-18, 18, 4.5)$, respectively. Transverse slices of the phantom corresponding to the planes $z = 1.91$, 0, and -1.69 are shown in Figs. 6(a), 6(b), and 6(c), respectively. A 3D scanning geometry was employed in which the incident wave-field direction $\mathbf{s}_0$ and x–y detector planes at $z = d$ and $z = d + \Delta$ were rotated simultaneously through a 2π angular range about the z axis. The probing spherical wave had a wavelength of $\lambda = 2.5 \times 10^{-4}$ (arbitrary units), and the two-dimensional detector arrays in the $z = d$ and $z = d + \Delta$ planes were of dimension of 20×20 and contained 1024×1024 elements. Two measurement configurations were considered that had $(d = 100, \Delta = 4, z_0 = 96.08, z_0' = 99.92)$ and $(d = 100, \Delta = 16, z_0 = 96.08, z_0' = 111.45)$. These will be referred to as spherical-wave geometries one and two, respectively. Note that both of these configurations result in $\alpha = 0.7$. We also considered a plane-wave case ($\alpha = 1$) for which $(d = 100, \Delta = 4)$.

The complex phases $\psi(x, y; z)$ on the detector arrays were calculated analytically by use of Eqs. (22) and (23), and the intensity functions at each tomographic view angle were formed as $I(x, y; z) = \exp[\psi(x, y; z) + \psi^*(x, y; z)]$. The simulated intensities $I(x, y; d)$ and $I(x, y; d + \Delta)$ were calculated at 128 evenly spaced view angles over the interval $[0, 2\pi)$. Note that the phantom objects were, by construction, weakly scattering objects. The deleterious effects of strong scattering in linearized DT are well known[11,12] and are not investigated in this paper.

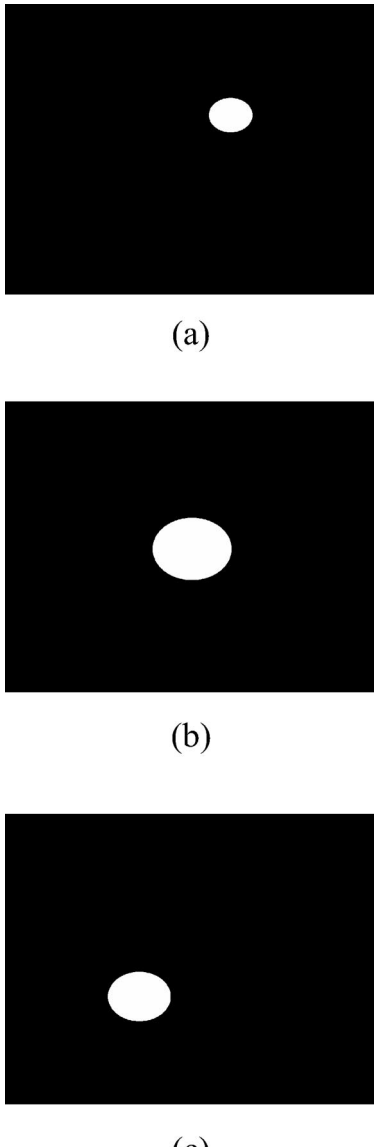

Fig. 6. The $z = 1.91$, 0, and -1.69 planes of the simulated 3D scattering potential.

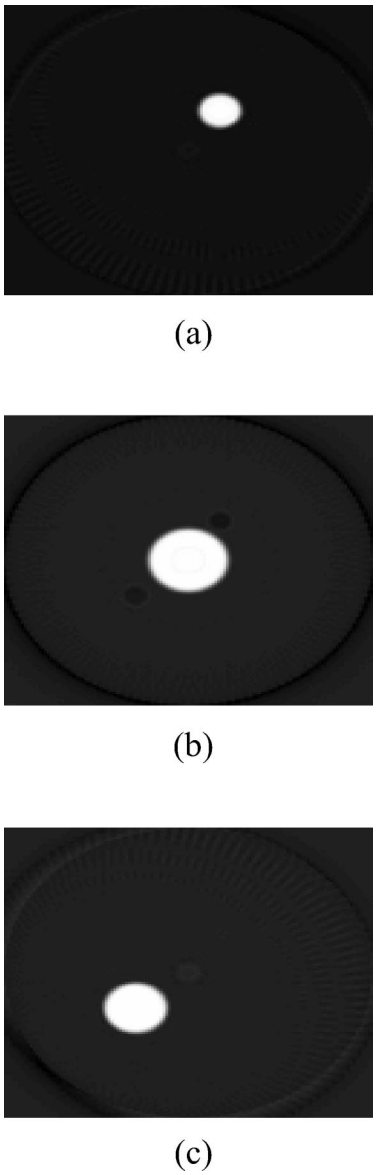

Fig. 7. Noiseless reconstructions of the $z = 1.91$, 0, and -1.69 planes obtained by use of the plane-wave I-DT method ($\alpha = 1$).

To investigate the noise-propagation properties of the reconstruction method, we treated the intensity data as realizations of an uncorrelated Gaussian stochastic process that was characterized by its mean μ and standard deviation σ. In generating the noisy data, μ was set equal to the noiseless value of $I(x, y; z)$ at a given detector location and σ was chosen to satisfy $\sigma/\mu = 0.1\%$.

B. Reconstruction Procedure

From the simulated intensity measurements, we formed $D_S(x, y; d, z_0)$ and $D_S(x, y; d + \Delta, z_0')$ according to Eq. (25), and used Eq. (29) to estimate $\tilde{F}[u/\alpha^2, v/\alpha^2, (w_\alpha - k)]$ for components $(u, v) \neq (0, 0)$ that have smaller values than those defined by the $n = 1$ case of Eq. (30). From the determined values of $\tilde{F}[u/\alpha^2, v/\alpha^2, (w_\alpha - k)]$, a low-pass-filtered approximation of $F(\mathbf{r})$ was reconstructed by use of the reconstruction algorithm for spherical-wave DT that is described in Ref. 13.

C. Reconstructed Images

Figures 7 and 8 contain reconstructions of the $z = 1.91$, 0, and -1.69 transverse slices that were obtained from the noiseless measurement data corresponding to the plane-wave geometry ($\alpha = 1$) and spherical-wave geometry one ($\alpha = 0.7, \Delta = 4$), respectively. As expected, both the plane-wave and the spherical-wave I-DT reconstruction methods produced low-pass-filtered images that resemble closely the true phantom slices shown in Fig. 6.

Figures 9 and 10 contain images of the same transverse slices that were reconstructed from the noisy measurement data corresponding to spherical-wave geometries one ($\alpha = 0.7, \Delta = 4$) and two ($\alpha = 0.7, \Delta = 16$), respectively. It is to be noted that the images in Fig. 9 have a noisier appearance than those in Fig. 10. Specifically, the images contained in Fig. 9 have more non-uniform backgrounds than those contained in Fig. 10. This is consistent with our assertion that the variance of the low-

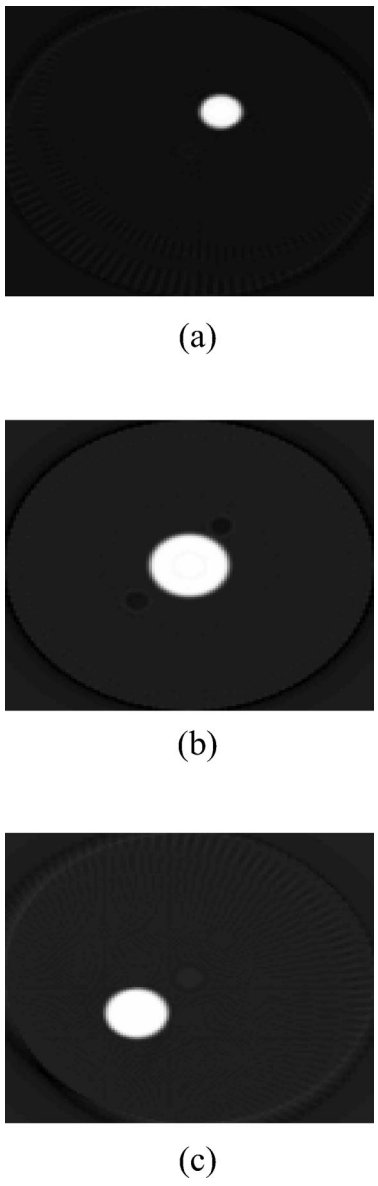

Fig. 8. Noiseless reconstructions of the $z = 1.91$, 0, and -1.69 planes obtained by use of the spherical-wave I-DT method with geometry one ($\alpha = 0.7, \Delta = 4$).

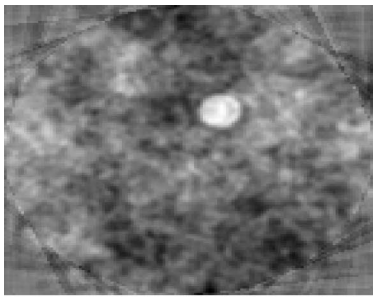

(a)

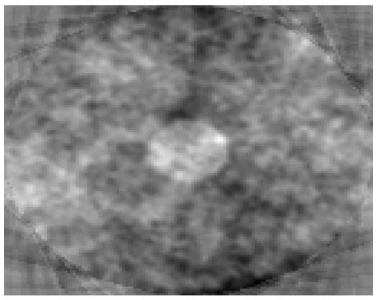

(b)

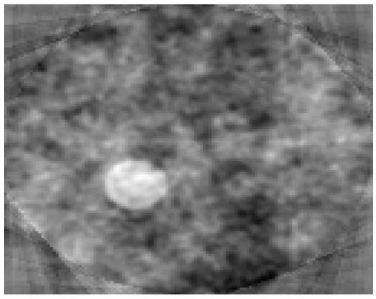

(c)

Fig. 9. Noisy reconstructions of the $z = 1.91$, 0, and -1.69 planes obtained by use of the spherical-wave I-DT method with geometry one ($\alpha = 0.7, \Delta = 4$).

frequency components of $\tilde{F}$ can be reduced by increasing the detector plane spacing Δ of the measurement geometry.

6. SUMMARY

Although DT is a well-established imaging method, it has the undesirable feature that it requires knowledge of both the magnitude and the phase of the measured fields, which can pose experimental difficulties in optical applications. Because of this, the success of DT imaging in optical applications has been limited. A new theory of I-DT using plane-wave incident fields has been proposed recently[2,3] that replaces explicit phase measurements by (two) intensity measurements taken in different parallel planes at each tomographic view angle. In many practical experiments, however, a measurement geometry may be employed in which the probing field is a spherical wave produced by a point source located a finite distance away from the scatterer. Under certain assumptions regarding the placement of the point source and the detector plane, a spherical-wave DT reconstruction method was developed previously.[4] However, this method requires knowledge of the magnitude and phase of the measured fields.

In this work we derived a reconstruction method for spherical-wave I-DT. In accomplishing this, we employed the same assumptions about the measurement geometry and object that were used in the spherical-wave DT formulation. As in the plane-wave I-DT method, explicit phase measurements are replaced by measurements of the diffracted-wave-field intensity on different parallel planes at each tomographic view angle. To obtain a simple spherical-wave I-DT reconstruction method that is similar in structure to the plane-wave I-DT reconstruction method, we showed that the source position must be varied in a specific way between intensity mea-

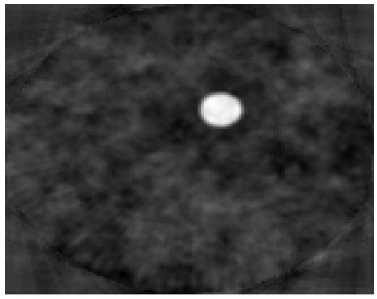

(a)

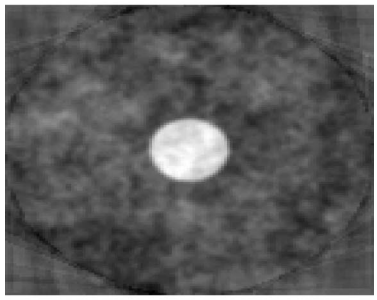

(b)

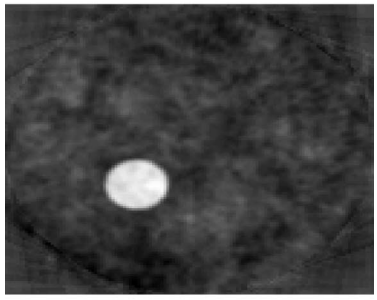

(c)

Fig. 10. Noisy reconstructions of the $z = 1.91$, 0, and -1.69 planes obtained by use of the spherical-wave I-DT method with geometry two ($\alpha = 0.7, \Delta = 16$).

surements on the (two) detector planes at each view angle. The reconstruction method was implemented numerically and employed successfully for reconstruction of noiseless and noisy images of a simulated 3D weak-scattering object.

APPENDIX A: DETERMINATION OF $\tilde{F}(K)$ WITH A FIXED SOURCE–OBJECT SPACING

With a fixed spacing between the spherical-wave source and the scattering object, reconstruction of the Fourier components of the scattering potential can be accomplished by a careful mixing of data from multiple measurement directions. In this appendix we discuss how such reconstructions could be accomplished, at least in principle.

We begin by assuming that measurements of the scattered intensity have been taken on two measurement planes, situated at distances $z = d$ and $z = d + \Delta$ for all directions of incidence of the scattered field. Measurements taken at the inner measurement distance will be referred to as a measurement on plane 1; likewise, measurements taken at the outer distance will be referred to as a measurement on plane 2. The value of α on a given measurement plane will be referenced with a subscript; i.e., the value of α on plane 2 is referred to by α_2. We will consider intensity measurements for four directions of incidence, to be denoted $\mathbf{s}^{(i)}$, where $i = a, b, c, d$.

Let us first consider the information contained in an intensity measurement on a single measurement plane for a single direction of incidence. We have seen (recall Fig. 5) that such an intensity measurement contains information about the components of $\tilde{F}$ on a semi-ellipse whose axes are dictated by the value of α. In particular, a single Fourier component of the intensity data function in the measurement plane is a linear sum of Fourier components of the scattering potential located at a pair of coordinates on opposite sides of the ellipse, as seen in Eq. (26); we denote the directions of the wave vectors of these components by $\mathbf{q}^{(i)}$ and $\tilde{\mathbf{q}}^{(i)}$, where $i = a, b, c, d$ refers to the direction of incidence being considered [see Fig. 11(a)]. The half-angle θ_i between the two complimentary wave vectors is readily found to be given by

$$\theta_i = \tan^{-1}\left[\frac{\sqrt{u_i^2 + v_i^2}/\alpha_j^2}{\sqrt{k^2 - (u_i/\alpha_j)^2 - (v_i/\alpha_j)^2} - k}\right], \quad \text{(A1)}$$

where u_i, v_i are the selected transverse Fourier components for the ith measurement and $j = 1, 2$ refers to the measurement plane used to make the measurement. Furthermore, the length L_i of each of these wave vectors is given by

$$L_i = u_i^2/\alpha_j^4 + v_i^2/\alpha_j^4 + (w_{\alpha_j} - k)^2. \quad \text{(A2)}$$

It is to be noted from this expression that Fourier components taken from different measurement planes can be found with equal lengths, because even though $\alpha_1 \neq \alpha_2$, we are free to select a u_1, v_1 and u_2, v_2 such that $L_1 = L_2$.

We now consider how to determine the component of $\tilde{F}$ with wave vector $\mathbf{q}^{(a)}$. We consider four intensity measurements with Fourier components arranged as in Fig. 11(b). The intensity measurements in directions a and c are taken on plane 1, and the measurements in directions b and d are taken on plane 2. The lengths of all Fourier components are taken to be equal; this can be done by an appropriate choice of the transverse components of the wave vectors for the two measurement planes.

The result of this arrangement is that we end up with four linear equations [the relations between the intensity and the components of $\tilde{F}$ for four measurements, all derived from Eq. (26)] and four unknowns [the components of $\tilde{F}(\mathbf{q}^{(i)})$]. We may therefore solve for the component of $\tilde{F}$ with wave vector $\mathbf{q}^{(a)}$.

Although this reconstruction procedure requires four intensity measurements for reconstruction of a component of $\tilde{F}$, the solution to the system of equations that follows results in the determination of $\tilde{F}$ for four wave vectors ($\mathbf{q}^{(a)}$, $\mathbf{q}^{(b)}$, $\mathbf{q}^{(c)}$, and $\mathbf{q}^{(d)}$). This is similar to the case for the plane-wave I-DT, in which two components of the scattering potential can be determined from two intensity measurements. It might be said that the reconstruction of the scattering potential requires a "presorting" of the intensity data set before the Fourier components of $\tilde{F}$ may be determined. An exact way of performing such a presorting, however, is not yet known.

The series of equations derived by use of this method will have a solution if and only if the determinant of the coefficients is nonzero. It can be shown after some calculation that this determinant is given by

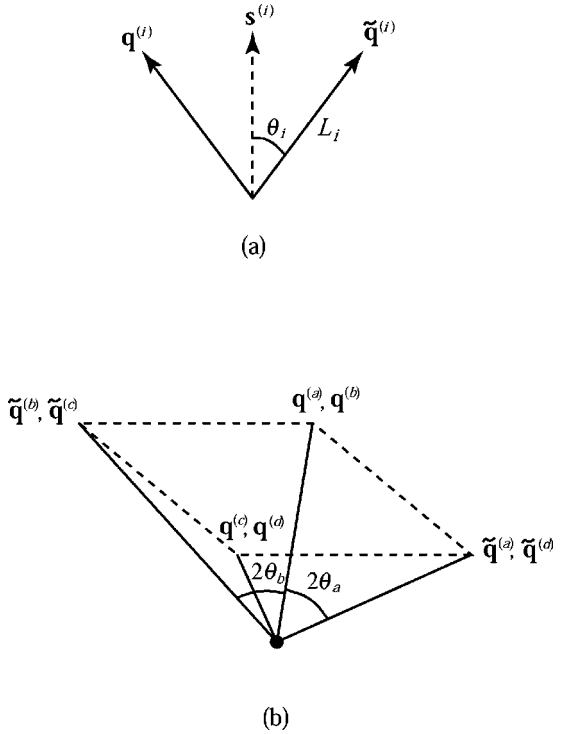

Fig. 11. Illustration of (a) the wave vectors of the scattering potential, that are mixed together in a single intensity measurement and (b) a four-measurement arrangement used to extract a component of the scattering potential.

$$\mathrm{Det} = \frac{2(2\pi)^8}{z_0^4 w_{\alpha_1}^2 w_{\alpha_2}^2 \alpha_1^4 \alpha_2^4} \times \sin[2(w_{\alpha_1} - w_{\alpha_2})d + 2(w_{\alpha_2} - k)\Delta]. \tag{A3}$$

This term is comparable to the factor which appears in the original I-DT formula [see, for instance, Eq. (12) of Ref. 3].

*Present address, Department of Physics and Optical Science, University of North Carolina at Charlotte, 9201 University City Boulevard, Charlotte, North Carolina 28223. Phone, 704-687-4511; e-mail, gjgbur@uncc.edu.

REFERENCES

1. E. Wolf, "Principles and development of diffraction tomography," in *Trends in Optics*, A. Consortini, ed. (Academic, San Diego, Calif., 1996), pp. 83–110.
2. G. Gbur and E. Wolf, "Hybrid diffraction tomography without phase information," J. Opt. Soc. Am. A **19**, 2194–2202 (2002).
3. G. Gbur and E. Wolf, "Diffraction tomography without phase information," Opt. Lett. **27**, 1890–1892 (2002).
4. A. J. Devaney, "Generalized projection-slice theorem for fan beam diffraction tomography," Ultrason. Imaging **7**, 264–275 (1985).
5. M. Born and E. Wolf, *Principles of Optics*, 7th ed. (Cambridge U. Press, Cambridge, UK, 1999).
6. L. Mandel and E. Wolf, *Optical Coherence and Quantum Optics* (Cambridge U. Press, Cambridge, UK, 1995).
7. A. J. Devaney, "Diffraction tomography," in *Inverse Methods in Electromagnetic Imaging, Part 2*, W. M. Boerner, H. Brand, L. A. Cram, D. T. Gjessing, A. K. Jordan, W. Keydel, G. Schwierz, and M. Vogel, eds. (Reidel, Boston, Mass., 1985), pp. 1107–1135.
8. M. A. Anastasio and X. Pan, "Computationally efficient and statistically robust image reconstruction in three-dimensional diffraction tomography," J. Opt. Soc. Am. A **17**, 391–400 (2000).
9. M. R. Teague, "Deterministic phase retrieval: a Green's function solution," J. Opt. Soc. Am. **73**, 1434–1441 (1983).
10. G. Gbur and E. Wolf, "The information content of the scattered intensity in diffraction tomography," Info. Sci. **162**, 3–20 (2004).
11. M. Slaney, A. Kak, and L. Larsen, "Limitations of imaging with first-order diffraction tomography," IEEE Trans. Microwave Theory Tech. **32**, 860–874 (1984).
12. B. Chen and J. J. Stamnes, "Validity of diffraction tomography based on the first-Born and first-Rytov approximations," Appl. Opt. **37**, 2996–3006 (1998).
13. M. A. Anastasio and X. Pan, "An improved reconstruction algorithm for 3D diffraction tomography using spherical-wave sources," IEEE Trans. Biomed. Eng. **50**, 517–521 (2003).